LETTER

doi:10.1038/nature23003

Personalized RNA mutanome vaccines mobilize poly-specific therapeutic immunity against cancer

Ugur Sahin[1,2,3], Evelyna Derhovanessian[1], Matthias Miller[1], Björn-Philipp Kloke[1], Petra Simon[1], Martin Löwer[2], Valesca Bukur[1,2], Arbel D. Tadmor[2], Ulrich Luxemburger[1], Barbara Schrörs[2], Tana Omokoko[1], Mathias Vormehr[1,3], Christian Albrecht[2], Anna Paruzynski[1], Andreas N. Kuhn[1], Janina Buck[1], Sandra Heesch[1], Katharina H. Schreeb[1], Felicitas Müller[1], Inga Ortseifer[1], Isabel Vogler[1], Eva Godehardt[1], Sebastian Attig[2,3], Richard Rae[2], Andrea Breitkreuz[1], Claudia Tolliver[1], Martin Suchan[2], Goran Martic[2], Alexander Hohberger[3], Patrick Sorn[2], Jan Diekmann[1], Janko Ciesla[4], Olga Waksmann[4], Alexandra-Kemmer Brück[1], Meike Witt[1], Martina Zillgen[1], Andree Rothermel[2], Barbara Kasemann[2], David Langer[1], Stefanie Bolte[1], Mustafa Diken[1,2], Sebastian Kreiter[1,2], Romina Nemecek[5], Christoffer Gebhardt[6,7], Stephan Grabbe[3], Christoph Höller[5], Jochen Utikal[6,7], Christoph Huber[1,2,3], Carmen Loquai[3]* & Özlem Türeci[8]*

T cells directed against mutant neo-epitopes drive cancer immunity. However, spontaneous immune recognition of mutations is inefficient. We recently introduced the concept of individualized mutanome vaccines and implemented an RNA-based poly-neo-epitope approach to mobilize immunity against a spectrum of cancer mutations[1,2]. Here we report the first-in-human application of this concept in melanoma. We set up a process comprising comprehensive identification of individual mutations, computational prediction of neo-epitopes, and design and manufacturing of a vaccine unique for each patient. All patients developed T cell responses against multiple vaccine neo-epitopes at up to high single-digit percentages. Vaccine-induced T cell infiltration and neo-epitope-specific killing of autologous tumour cells were shown in post-vaccination resected metastases from two patients. The cumulative rate of metastatic events was highly significantly reduced after the start of vaccination, resulting in a sustained progression-free survival. Two of the five patients with metastatic disease experienced vaccine-related objective responses. One of these patients had a late relapse owing to outgrowth of β2-microglobulin-deficient melanoma cells as an acquired resistance mechanism. A third patient developed a complete response to vaccination in combination with PD-1 blockade therapy. Our study demonstrates that individual mutations can be exploited, thereby opening a path to personalized immunotherapy for patients with cancer.

Cancer mutations can form neo-epitopes recognized by T cells on HLA molecules, which contributes to the clinical success of immunotherapy[3–7]. Only a small fraction of mutations induce spontaneous immune responses in the tumour-bearing host, which limits immunotherapy efficacy to tumours with a high mutational load[8–10]. In mouse vaccination models, a substantial fraction of cancer mutations is immunogenic and preferably recognized by $CD4^+$ T cells[2]. Vaccines composed of predicted HLA class II[2] and class I neo-epitopes[11,12] have previously been shown to induce rejection of mouse tumours. Altogether, these findings created enthusiasm for neo-epitope vaccines[13,14]. As the vast majority of cancer mutations are unique to the individual patient, personalized approaches are needed. For the first-in-human testing of such an approach, we developed a process compliant with regulatory requirements (Fig. 1a). Non-synonymous mutations expressed by thirteen patients with stage III and IV melanoma were identified by comparative exome and RNA sequencing of routine tumour biopsies and healthy blood cells. Mutations were ranked according to: (1) predicted high-affinity binding to autologous HLA class II and high expression of the mutation-encoding RNA[2], and (2) predicted HLA class I binding. Ten selected mutations per patient (five for patient P09) were engineered into two synthetic RNAs, each encoding five linker-connected 27mer peptides with the mutation in position 14 (pentatope RNAs) (Fig. 1b, Supplementary Table 1). RNA was produced within 68 days (range 49 to 102 days) according to good manufacturing practice with a success rate of 100% (Fig. 1c). Analytical testing extended the median time from selection of mutations to vaccine release to 103 days (range 89 to 160 days). Patients with NY-ESO-1- and/or tyrosinase-positive melanoma received an RNA vaccine encoding these shared tumour-associated self-antigens until release of their neo-epitope vaccine. At least eight doses of the neo-epitope vaccine were injected percutaneously into inguinal lymph nodes under ultrasound control (Fig. 1d). Previously, in mouse models, we showed efficient uptake, translation of RNA-encoded antigens by lymph-node-resident dendritic cells (DCs), and intrinsic adjuvant activity[15].

All patients completed treatment with a maximum of 20 neo-epitope vaccine doses (Extended Data Table 1), which they tolerated well without related serious adverse events. The immunogenicity of each of the 125 mutations administered in this study was analysed by IFNγ ELISpot in $CD4^+$ and $CD8^+$ T cells in pre- and post-vaccination blood samples (Supplementary Table 2). Responses were detected against 60% of the predicted neo-epitopes (Fig. 1e, Extended Data Table 2), and each patient developed T cells against at least three mutations. Pre-existing weak responses against one-third of the immunogenic neo-epitopes were augmented upon vaccination (Fig. 1e, f, Extended Data Fig. 2a). The other two-thirds were *de novo* responses. Immunogenic mutations were evenly distributed across the five positions of the pentatope RNA (Fig. 1g), indicating lack of positional bias. As previously observed in mice[2], the majority of neo-epitopes mounted exclusively $CD4^+$ responses (Fig. 1e, Extended Data Fig. 2b). A smaller fraction was recognized by $CD8^+$ cytotoxic lymphocytes (CTLs) only. One-quarter showed concomitant $CD4^+$ and $CD8^+$ responses, recognizing different regions of the mutated 27mer sequence (Fig. 1e, Extended Data Fig. 2c, d).

Immune tolerance is expected to suppress T cell responses against broadly expressed proteins. In fact, the majority of neo-epitope-

[1]Biopharmaceutical New Technologies (BioNTech) Corporation, An der Goldgrube 12, 55131 Mainz, Germany. [2]TRON – Translational Oncology at the University Medical Center of Johannes Gutenberg University gGmbH, Freiligrathstraße 12, 55131 Mainz, Germany. [3]University Medical Center of the Johannes Gutenberg University, Langenbeckstraße 1, 55131 Mainz, Germany. [4]EUFETS GmbH, Vollmersbachstraße 66, 55743 Idar-Oberstein, Germany. [5]Medical University of Vienna, Spitalgasse 23, 1090 Vienna, Austria. [6]German Cancer Research Center (DKFZ), Im Neuenheimer Feld 280, 69120 Heidelberg, Germany. [7]University Medical Center Mannheim, Heidelberg University, Theodor-Kutzer-Ufer 1-3, 68135 Mannheim, Germany. [8]CI3 - Cluster for Individualized Immunointervention e.V, Hölderlinstraße 8, 55131 Mainz, Germany.
*These authors contributed equally to this work.

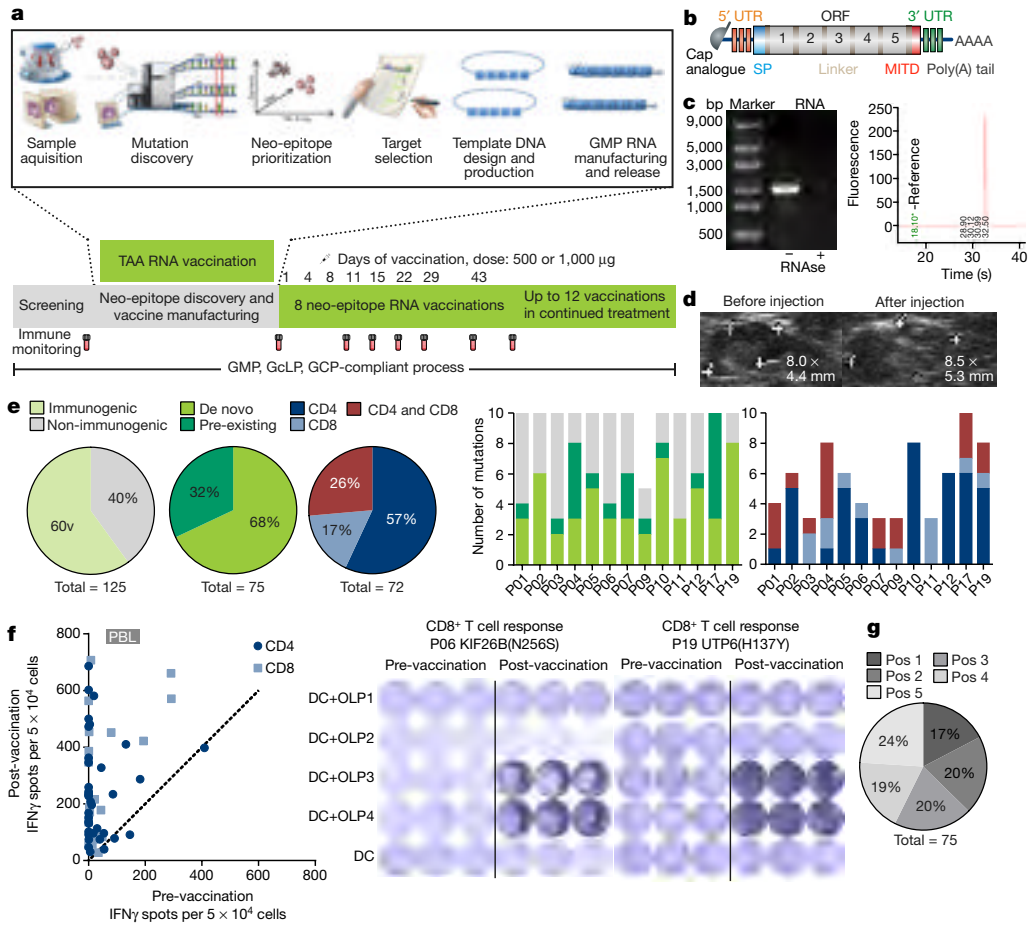

Figure 1 | Broad mobilization of mutation-specific immunity by vaccination. a, Vaccine design, manufacturing and clinical study procedure. TAA, tumour-associated self-antigen. **b**, Two synthetic pharmacologically optimized RNA molecules per patient, each with five mutations (pentatope RNA). **c**, Denaturing agarose gel and microfluidic capillary electrophoresis of RNA. **d**, Ultrasound-guided percutaneous vaccine injection into lymph nodes. **e**–**g**, Characterization of $CD4^+$ and $CD8^+$ T cells after *in vitro* stimulation with pentatope-RNA-transfected autologous irradiated CD8/CD4-depleted PBMCs in ELISpot assays read-out on autologous DCs. **e**, T cell response statistics for all 125 mutations on cohort level (pie charts) or per individual patient (bar charts). **f**, Pre- versus post-vaccination responses to DCs loaded with one of the four overlapping 15mer peptides (OLPs) of the respective neo-epitope for 10 patients (left) or examples (right). **g**, Positions of immunogenic neo-epitopes within the pentatope RNA. Control RNA, luciferase; UTR, untranslated region; ORF, open reading frame; SP, signal peptide; MITD, MHC class I trafficking domain.

vaccine-induced responses did not or only weakly cross-reacted with autologous DCs transfected with the RNA-encoded wild-type epitope (Fig. 1g, Extended Data Fig. 2e). Characterization of stronger wild-type cross-reactive responses indicated recognition of artificial epitopes not presented by normal cells (Extended Data Fig. 2f–g). Moreover, we found that wild-type cross-reactive responses represented mixed populations, including T cells, which recognize exclusively the mutated epitope (Extended Data Figs 2h, 3g).

Responses against one-fifth of the immunogenic mutations were detectable in blood without *in vitro* stimulation (Fig. 2a). In patients vaccinated with neo-epitopes and shared tumour-associated self-antigens, neo-epitope responses were stronger (Fig. 2b), probably owing to the lack of central immune tolerance.

For molecular characterization, we cloned neo-epitope-specific T cell receptor (TCR) α/β chains from single cells and co-transfected them into T cells for functional characterization. Moreover, for 13 of the reactivities we determined the actual recognized HLA class I ligands within the mutated sequence stretch to enable HLA multimer studies (Extended Data Table 3). TCR-β sequences of eight TCRs cloned from neo-epitope-specific $CD4^+$ and $CD8^+$ T cells of two patients (Fig. 2c, Extended Data Fig. 3, Extended Data Table 4) were not detectable in TCR deep-sequencing data of pre-vaccination blood samples from the patients, but were abundant in post-vaccination samples (Fig. 2d), confirming *de novo* priming of CTLs.

Neo-epitope-specific $CD8^+$ T cells expanded within 2–4 weeks to up to high single-digit percentages, as shown in several patients by *ex vivo* HLA multimer blood analysis (Fig. 2e). T cells had a weakly PD-1^+, central- or effector-memory phenotype and were fully functional with concomitant expression of IFNγ and TNFα (Fig. 2f) on antigen stimulation.

The patients had a recent history of recurrent disease and a high risk of relapse (Fig. 3a, top, Extended Data Table 5). Comparison of documented melanoma recurrences in all patients before and after neo-epitope vaccination (Fig. 3a, bottom left) showed a highly significant reduction of longitudinal cumulative recurrent metastatic events ($P < 0.0001$), translating into sustained progression-free survival (Fig. 3a, bottom right).

Eight patients had no radiologically detectable lesions at start of neo-epitope vaccination (Fig. 3a, top). These patients mounted strong immune responses (Fig. 1e, Extended Data Fig. 4a) and remained recurrence-free for the whole follow-up period (12 to 23 months). The other five patients experienced melanoma relapses shortly after inclusion and, despite initiation of standard treatment, had progressing metastases at start of their neo-epitope vaccination. Of these, patient 03 (P03) and P04 developed neo-epitope-vaccine-related objective clinical responses. P03 exhibited a complete response of multiple progressing metastases unresponsive to local radiotherapy and CTLA-4 blockade, and remained relapse-free for 26 months. P04 had a vaccine-related

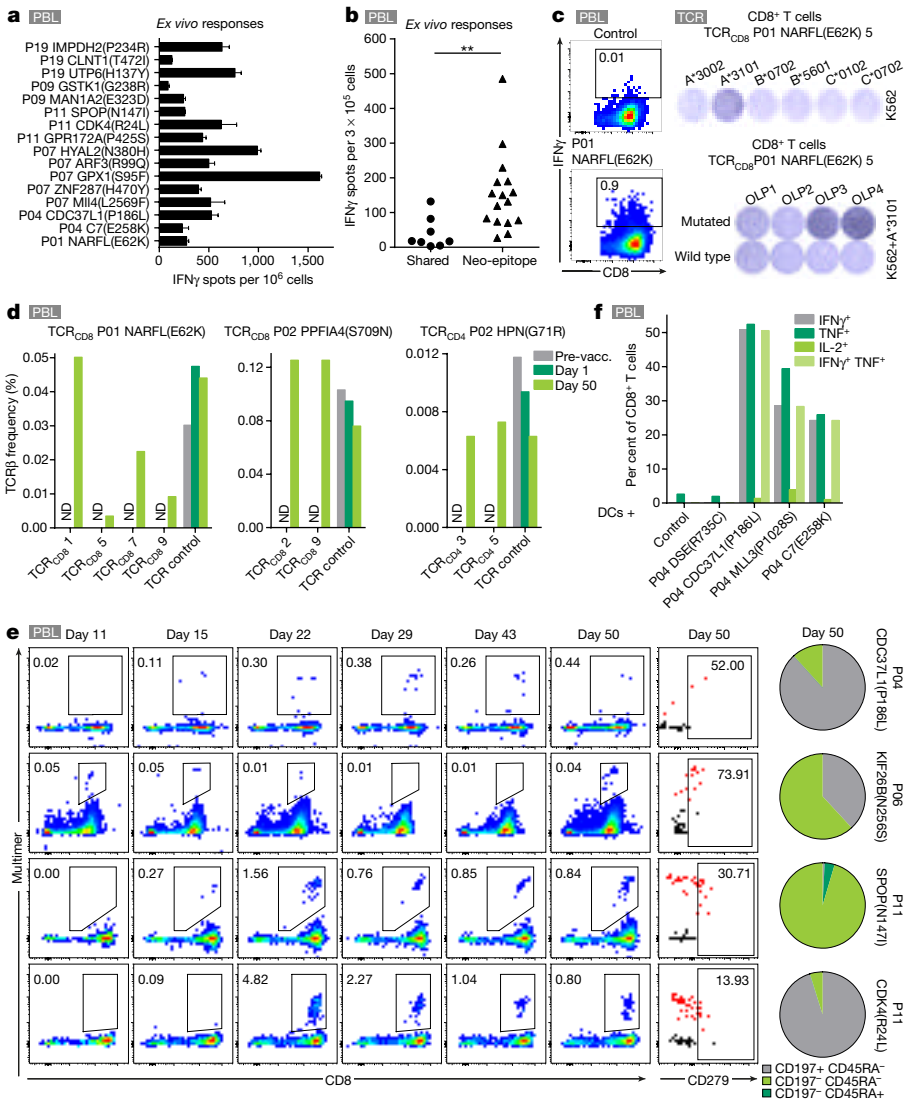

Figure 2 | Rapid expansion of neo-epitope-specific T cells with central and effector memory phenotypes by vaccination. **a**, **b**, PBMCs read-out without previous expansion against neo-epitope-RNA-loaded autologous DCs in ELISpot. Mann–Whitney test (**$P = 0.0017$). **c**, Activation-induced IFNγ -secretion-based single-cell sorting of CD8$^+$ T cells after *in vitro* stimulation with neo-epitope-RNA-loaded autologous DCs for TCR cloning. Control, luciferase RNA. Healthy-donor-derived CD8$^+$ T cells co-transfected with RNAs encoding the identified TCR-α /β chains tested on peptide-pulsed K562 cells expressing the patient's individual HLA alleles. **d**, Frequencies of neo-antigen-specific TCRs. ND, not detectable; TCR control, irrelevant-T-cell-derived TCR-β sequence. **e**, Kinetics and phenotype of selected CD8$^+$ T cell responses. PBMCs stained with neo-epitope-specific multimers (left). See also Extended Data Fig. 4b, c, g for specificity of selected dextramers. PBMCs stained for CD279 (PD-1) within the multimer-positive (red) and -negative (black) cell population (mid). Memory T cell subsets based on CD45RA and CD197 expression (right). **f**, Intracellular cytokine staining of CD8$^+$ T cells co-cultured with RNA-transfected DCs. Control, DCs without RNA.

partial response of abdominal lymph node metastases. P02 had a slowly progressing multi-metastatic disease under BRAF inhibitor treatment and developed a mixed response upon adding neo-epitope vaccine. P17 had an axillar lymph node metastasis that remained stable after the start of neo-epitope vaccination. It was removed after four vaccine injections and used to generate tumour infiltrating lymphocytes (TILs) and a melanoma cell line. P07 developed complete response in combination with PD-1 blockade.

Three patients provided further insights into neo-epitope vaccine effects. P07 experienced multiple relapses with shortening relapse-free intervals and progressing metastases at the start of neo-epitope vaccination. Owing to fast disease progression despite a strong response against six neo-antigens (five measurable *ex vivo,* Figs 1e, 2a), vaccination was discontinued and P07 entered a compassionate anti-PD-1 (pembrolizumab) treatment program. The patient experienced 80% reduction in size of multiple melanoma lesions within two months and eventually a complete response (Fig. 3b). Vaccine-induced T cells persisted for up to 9 months after the end of vaccination (Fig. 3c).

P17 had responses against all ten vaccine-encoded mutations in post-vaccine TILs and in peripheral blood mononuclear cells (PBMCs) (Figs 1e, 3d). In the TILs, we confirmed reactivity against retinol saturase RETSAT(P546S) and identified the HLA-A*6801-restricted ligand derived from this mutation (Fig. 3e). Characterization of the RETSAT(P546S)-specific TCR#8 identified from TILs by single-cell cloning (Fig. 3f, g) unexpectedly showed HLA-B*3701-restricted recognition of a different ligand derived from the same mutation (Fig. 3g, h, Extended Data Fig. 4d–f). TCR#8 conferred efficient killing of the autologous melanoma cell line MZ-I-017 derived from the post-vaccination sample, but not of autologous APCs (Fig. 3i).

P04 was regarded as tumour-free on the basis of magnetic resonance imaging (MRI) scans conducted before initiation of neo-epitope vaccination. Follow-up MRI scans showed abdominal lymph node metastases missed at the baseline. As P04 had mounted responses against eight mutations and was stable (Fig. 1e, Extended Data Fig. 5a), vaccination was continued. After 12 applications, residual metastases were resected and pathologically diagnosed as almost completely necrotic. CD8$^+$ T cell infiltration, PD-L1 staining and expression of immune activation and inflammation markers was increased, as compared to the pre-vaccination melanoma specimen (Fig. 4a, b, Extended Data Fig. 5d, e). Two months after surgery, MRI scans revealed new abdominal and liver metastases. Anti-PD-1 (nivolumab) treatment was initiated, but the disease progressed rapidly and the patient died.

To understand this unexpected treatment failure, we revisited the immunological data. T cells transfected with TCRs from CD8$^+$ TILs directed against the mutated neo-epitopes FLNA(P639L) and CDC37L1(P183L) recognized the mutated sequences with high sensitivity (Extended Data Fig. 5b, c), whereas MZ-GaBa-018, the autologous melanoma cell line from the post-vaccination resectate, was not recognized (Fig. 4e).

MZ-GaBa-018 cells expressed HLA class II, but showed no constitutive or IFNγ-inducible HLA class I surface expression (Fig. 4c).

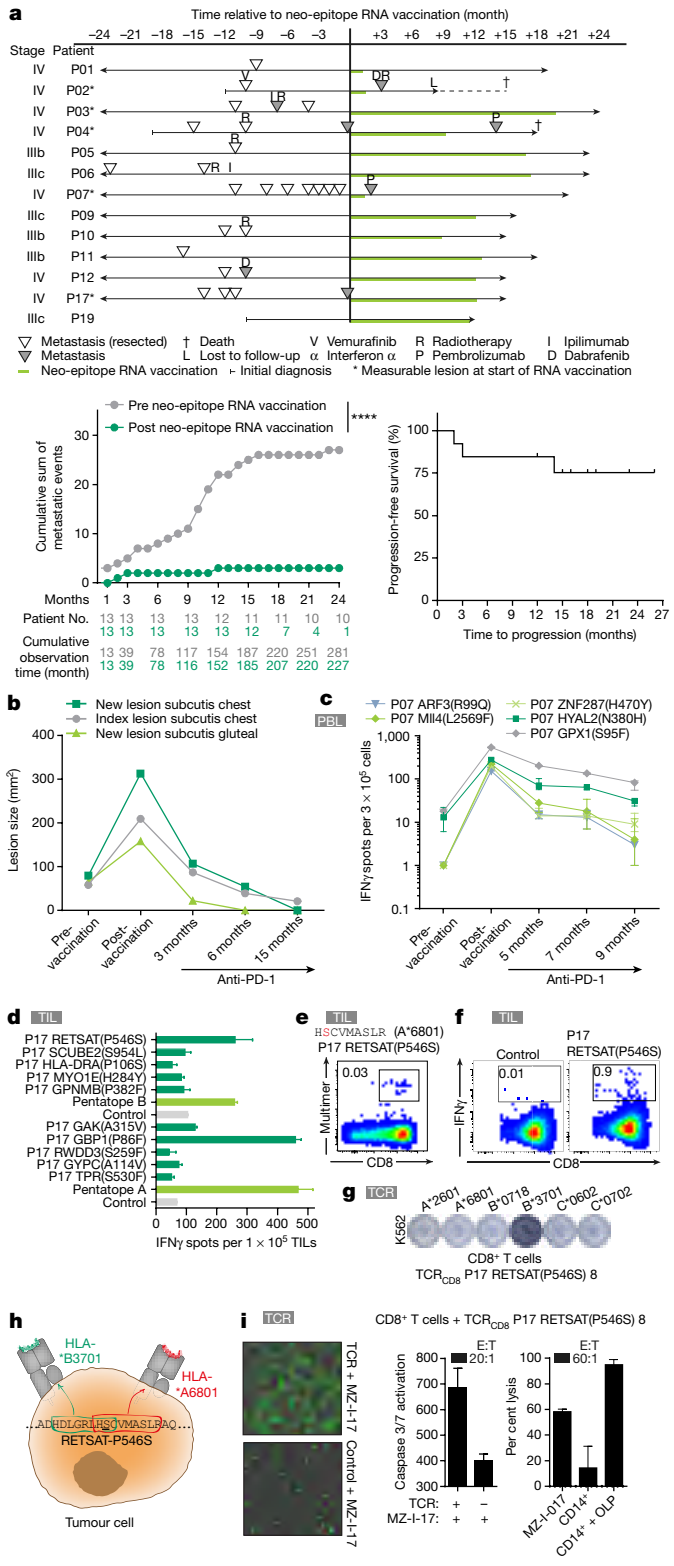

Figure 3 | Disease control by vaccination in melanoma patients with high risk of relapse. a, Recurrence and treatment (top) and progression-free survival (bottom, right) of patients. Cumulative sum of metastatic events per month before (grey) or after (green) neo-epitope RNA vaccination (bottom, left). Patient no., number of monitored patients. Fisher's exact test comparing the cumulative observation time without a metastatic event to the number of months with an event ($P < 0.0001$, (bottom, left)). **b**, **c**, Computer tomography of target lesions and vaccine-induced *ex vivo* responses by ELISpot for P07. **d**–**i**, Vaccine-induced T cell responses of P17. TILs and the tumour cell line MZ-I-17 derived from a lymph node metastasis resected after four RNA neo-epitope vaccinations. **d**, TIL reactivity against individual neo-epitopes **e**, HLA multimer staining of HLA-A*6801-restricted CD8$^+$ TILs recognizing a RETSAT(P546S) minimal epitope. **f**, IFNγ-secretion-based single-cell sorting of CD8$^+$ TILs for TCR cloning after co-culture with RNA-transfected DCs. Control, eGFP RNA. **g**–**i**, CD8$^+$ T cells expressing TCR#8 cloned from single TILs were tested for recognition of peptide-pulsed K562 cells transfected with individual HLA alleles of the patient by ELISpot (**g**) or for killing of P17-derived target cells by caspase 3/7 or luciferase cytotoxicity assays (**i**). Controls, CD8$^+$ T cells without TCR RNA (left); autologous CD14$^+$ cells ± OLPs (right). Results of triplicates (mean + s.d.). **h**, Neo-epitope presentation on two HLA-alleles.

HLA class I transcription was verified by next-generation sequencing (NGS) of MZ-GaBa-018 (RPKM values: HLA-A, 279; HLA-B, 207; HLA-C, 292), but not β2-microglobulin transcripts (RPKM = 0). Whole-exome sequencing revealed loss of both alleles of *B2M* and *TRIM69* genes by a deletion–inversion event (Fig. 4d, Extended Data Fig. 5f). Transfection of MZ-GaBa-018 with *B2M* RNA reconstituted HLA class I surface expression (Fig. 4c) and killing by T cells reprogrammed with the cloned neo-epitope-specific TCRs (Fig. 4e), as well as by autologous neo-epitope-RNA-stimulated blood-derived CD8$^+$ T cells (Extended Data Fig. 5g). Whereas the pre-treatment tumour sample of P04 stained almost homogenously for B2M, all tumour cells in the post-vaccine resectate were B2M-negative (Fig. 4f).

Overall, our findings illustrate that an unexpectedly broad repertoire of T cells is recruited by neo-epitope vaccination. Every patient, including individuals with relatively low mutational load, raised poly-specific immune responses. We found that one mutation may give rise to neo-epitopes either recognized concomitantly by CD4$^+$ and CD8$^+$ T cells or presented on different HLA class I restriction elements to different CD8$^+$ T cells. Likewise, the same neo-epitope–HLA combination was found to be recognized by neo-epitope-specific T cells with different TCR clonotypes (Extended Data Table 4).

Only a fraction of predicted high-affinity HLA class I binding mutant peptides are expected to be a naturally presented and immunogenic HLA class I ligand[11,16]. Accordingly, we observed CD8$^+$ responses against only 20 of 69 (29%) of predicted high-affinity class I binders. However, 12 of the 15 minimal CD8$^+$ neo-epitopes we identified have a good predicted binding affinity (Extended Data Table 3, Supplementary Tables 1, 2). Thus, despite its relatively low specificity, HLA class I neo-epitope prediction enables selection of strongly immunogenic ligands.

Likewise, HLA class II binding prediction correlated well with immunogenicity: 21 of 30 (70%), 30 of 67 (45%) and 9 of 26 (34%) of mutated sequences with a HLA class II binding score of <1, 1–10 or >10, respectively, induced CD4$^+$ responses. About 20% of the responses were raised against neo-epitopes with poor predicted HLA-binding scores, indicating the need for improvement of the sensitivity of our algorithms[16,17]. Post-vaccination biopsies from patients P04 and P17 enabled us to evaluate the effects of vaccine-induced immune responses on the patient's tumour. We confirmed infiltration of vaccine-induced neo-epitope-specific T cells in the respective tumours. We showed recognition and efficient killing of autologous melanoma cells but not autologous monocytes mediated by neo-epitope-specific TCRs. Collectively, these findings provide the complete chain of evidence proving that the neo-epitope vaccine executes its mode of action *in vivo*.

Our observations indicate that neo-epitope vaccines alone may prevent recurrent disease in high risk patients. Moreover, they provide a rationale for combining the vaccine with PD-1/PD-L1 blockade[18,19]. Neo-epitope-specific T cell subsets were PD-1$^+$ and of memory phenotype, and post-vaccine lesions were shown to upregulate PD-L1. Upon anti-PD-1 treatment after neo-epitope vaccination, P07 rapidly developed a complete response, the likelihood of which is otherwise reported to be below 10%[20].

Poly-neo-epitopic immunity reduces the risk of outgrowth of single neo-antigen loss variants[9], but complete loss of HLA class I presentation

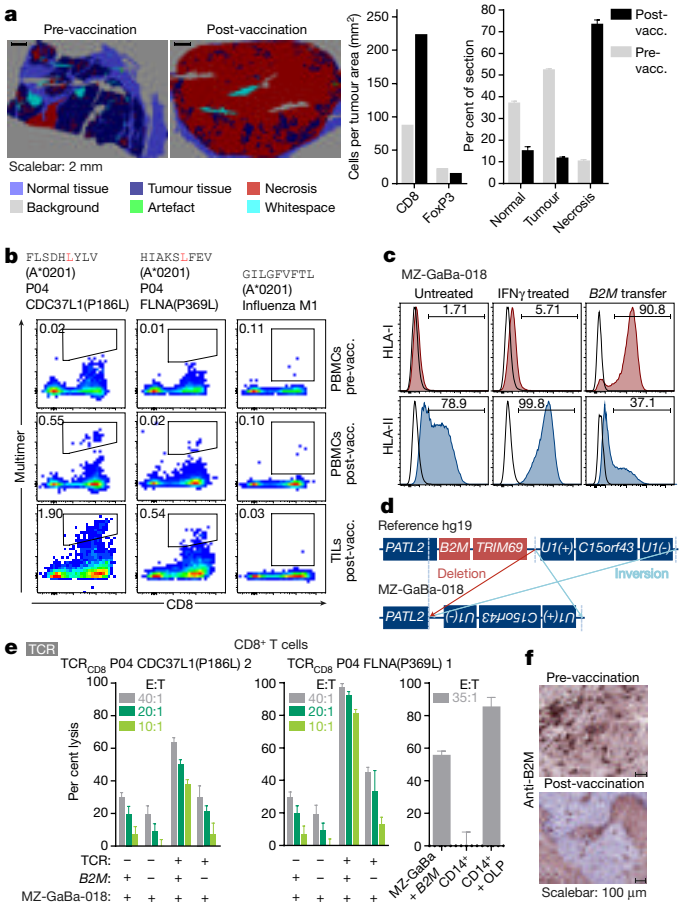

Figure 4 | Neo-epitope-induced CTL responses associated with immune escape by outgrowth of *B2M*-deficient melanoma cells in P04. **a**, Composition of metastases by computerized visualization and image-analysis-based quantification (right, mean + s.d. of triplicates). **b**, Frequency of CD8$^+$ T cells against two neo-epitopes in blood and TILs of a post-vaccination lesion detected by HLA multimers. Control, influenza M1 (A*0201). **c**, HLA surface expression of MZ-GaBa-018 under different conditions. **d**, Genomic mapping of the deletion and inversion event leading to B2M loss. **e**, Specific lysis of P04-derived target cells by neo-epitope TCR-transfected CD8$^+$ T cells measured by luciferase cytotoxicity assay. Controls: MZ-GaBa-018 cells without B2M transfer, CD8$^+$ T cells without TCR RNA (left and middle); autologous CD14$^+$ cells ± FLNA-P369L OLP (right). Results of triplicates (mean + s.d.). **f**, B2M staining of melanoma cells in pre- and post-vaccination metastases.

remains an effective escape mechanism[21]. The outgrowth of B2M-deficient tumour cells in the presence of poly-neo-epitope-specific immunity in P04 indicates that neo-epitope vaccines are potent enough to evoke the same resistance mechanisms as checkpoint blockade and adoptive T cell transfer[6,7,22]. This risk can be mitigated by combining mutanome vaccines with immunotherapies that do not rely on intact HLA class I presentation[23]. In summary, our study demonstrates the clinical feasibility, safety and antitumour activity of targeting individual cancer mutations by RNA neo-epitope vaccines, thereby supporting the case for making individually tailored medicines accessible to a wider range of patients.

Online Content Methods, along with any additional Extended Data display items and Source Data, are available in the online version of the paper; references unique to these sections appear only in the online paper.

Received 30 January; accepted 6 June 2017.
Published online 5 July 2017.

1. Castle, J. C. *et al.* Exploiting the mutanome for tumor vaccination. *Cancer Res.* **72,** 1081–1091 (2012).
2. Kreiter, S. *et al.* Mutant MHC class II epitopes drive therapeutic immune responses to cancer. *Nature* **520,** 692–696 (2015).
3. Rizvi, N. A. *et al.* Mutational landscape determines sensitivity to PD-1 blockade in non-small cell lung cancer. *Science* **348,** 124–128 (2015).
4. Snyder, A. *et al.* Genetic basis for clinical response to CTLA-4 blockade in melanoma. *N. Engl. J. Med.* **371,** 2189–2199 (2014).
5. Van Allen, E. M. *et al.* Genomic correlates of response to CTLA-4 blockade in metastatic melanoma. *Science* **350,** 207–211 (2015).
6. McGranahan, N. *et al.* Clonal neoantigens elicit T cell immunoreactivity and sensitivity to immune checkpoint blockade. *Science* **351,** 1463–1469 (2016).
7. Tran, E. *et al.* T-cell transfer therapy targeting mutant KRAS in cancer. *N. Engl. J. Med.* **375,** 2255–2262 (2016).
8. Linnemann, C. *et al.* High-throughput epitope discovery reveals frequent recognition of neo-antigens by CD4$^+$ T cells in human melanoma. *Nat. Med.* **21,** 81–85 (2015).
9. Matsushita, H. *et al.* Cancer exome analysis reveals a T-cell-dependent mechanism of cancer immunoediting. *Nature* **482,** 400–404 (2012).
10. Tran, E. *et al.* Immunogenicity of somatic mutations in human gastrointestinal cancers. *Science* **350,** 1387–1390 (2015).
11. Yadav, M. *et al.* Predicting immunogenic tumour mutations by combining mass spectrometry and exome sequencing. *Nature* **515,** 572–576 (2014).
12. Gubin, M. M. *et al.* Checkpoint blockade cancer immunotherapy targets tumour-specific mutant antigens. *Nature* **515,** 577–581 (2014).
13. Carreno, B. M. *et al.* Cancer immunotherapy. A dendritic cell vaccine increases the breadth and diversity of melanoma neoantigen-specific T cells. *Science* **348,** 803–808 (2015).
14. Delamarre, L., Mellman, I. & Yadav, M. Cancer immunotherapy. *Neo approaches to cancer vaccines. Science* **348,** 760–761 (2015).
15. Kreiter, S. *et al.* Intranodal vaccination with naked antigen-encoding RNA elicits potent prophylactic and therapeutic antitumoral immunity. *Cancer Res.* **70,** 9031–9040 (2010).
16. Bassani-Sternberg, M. *et al.* Direct identification of clinically relevant neoepitopes presented on native human melanoma tissue by mass spectrometry. *Nat. Commun.* **7,** 13404 (2016).
17. Abelin, J. G. *et al.* Mass spectrometry profiling of HLA-associated peptidomes in mono-allelic cells enables more accurate epitope prediction. *Immunity* **46,** 315–326 (2017).
18. Chen, D. S. & Mellman, I. Elements of cancer immunity and the cancer-immune set point. *Nature* **541,** 321–330 (2017).
19. Tumeh, P. C. *et al.* PD-1 blockade induces responses by inhibiting adaptive immune resistance. *Nature* **515,** 568–571 (2014).
20. Robert, C. *et al.* Pembrolizumab versus ipilimumab in advanced melanoma. *N. Engl. J. Med.* **372,** 2521–2532 (2015).
21. D'Urso, C. M. *et al.* Lack of HLA class I antigen expression by cultured melanoma cells FO-1 due to a defect in B2m gene expression. *J. Clin. Invest.* **87,** 284–292 (1991).
22. Zaretsky, J. M. *et al.* Mutations associated with acquired resistance to PD-1 blockade in melanoma. *N. Engl. J. Med.* **375,** 819–829 (2016).
23. Melero, I. *et al.* Evolving synergistic combinations of targeted immunotherapies to combat cancer. *Nat. Rev. Cancer* **15,** 457–472 (2015).

Supplementary Information is available in the online version of the paper.

Acknowledgements We thank J. de Graaf, I. Eichelbrönner, L. Leppin, L. Giese and S. Vogler, D. Becker, M. Dorner, J. Grützner, M. Hossainzadeh, A. Selmi, S. Wessel, C. Ecker, M. Lochschmitt, B. Schmitz, C. Anft, N. Bidmon, H. Schröder, D. Barea Roldán, C. Walter, S. Wöll, C. Rohde, O. Renz, F. Bayer, C. Kröner, B. Otte, T. Stricker, M. Drude S. Petri, M. Mechler, L. Hebich, B. Steege, A. Oelbermann, J. Schwarz, C. Britten, J. C. Castle and B. Pless for technical support, project management and advice. We thank A. Tüttenberg for support with a figure. We thank I. Mellman, L. Delamarre and G. Fine for critical reading of the manuscript. We thank K. Sahin for her advice. The study was supported by the CI3 cluster program of the Federal Ministry of Education and Research (BMBF).

Author Contributions U.S. conceptualized the work and strategy. E.D., Pe.Si., T.O., I.O., I.V., S.A., A.R. and B.K. planned and analysed experiments. E.G., R.R., A.B., C.T. and A.H. did experiments. M.L., V.B., A.D.T., B.S., C.A., A.P. and Pa.So. performed and analysed NGS runs. A.N.K., J.B. and J.C. manufactured the RNA vaccines, O.W., M.W. and M.Z. performed quality assurance. M.M., B.K., S.H., K.H.S., F.M., A.K.-B., D.L. and S.B. managed sample logistics. R.N., C.G., S.G., C.H., J.U. are clinical investigators. C.L. is the principal clinical investigator. U.L., J.D., M.D. and S.K. supported clinical grade assays. U.S., ÖT supported by E.D., M.V., Pe.Si., M.L, M.M., B.S. interpreted data and wrote the manuscript. All authors supported the revision of the manuscript.

Author Information Reprints and permissions information is available at www.nature.com/reprints. The authors declare competing financial interests: details are available in the online version of the paper. Readers are welcome to comment on the online version of the paper. Publisher's note: Springer Nature remains neutral with regard to jurisdictional claims in published maps and institutional affiliations. Correspondence and requests for materials should be addressed to U.S. (sahin@uni-mainz.de).

Reviewer Information *Nature* thanks C. Melief and the other anonymous reviewer(s) for their contribution to the peer review of this work.

METHODS

Data reporting. No statistical methods were used to predetermine sample size. The experiments were not randomized and the investigators were not blinded to allocation during experiments and outcome assessment.

Study design. The main objectives of this multicentre phase I study (NCT02035956) were to assess safety of the vaccine and vaccine-induced antigen-specific immune responses.

The study was carried out in accordance with the Declaration of Helsinki and good clinical practice guidelines and with approval by the institutional review board or independent ethics committee of each participating site and the competent regulatory authorities. All patients provided written informed consent.

Eligible patients were ≥18 years old, and had malignant melanoma stage IIIA-C or IV (AJCC 2009 melanoma classification) in complete remission, partial remission or stable disease at any stage of treatment. Patients with metastases were eligible if they could be treated with an active compound until availability of their individualized vaccine. Patients required adequate haematological and end-organ function. Key exclusion criteria were clinically relevant autoimmune disease, HIV, HBV, HCV and acute EBV or CMV infections and brain metastases.

Regular treatment was eight injections within 43 days; continued treatment was left to the investigators' discretion. The RNA pentatopes were diluted in 1.0 mg ml^{-1} Ringer's solution (Rotexmedica or BAG Healthcare) and injected into separate inguinal lymph nodes. Ten patients were administered 500 μg and three patients 1,000 μg per treatment to explore two different dose ranges.

Key study assessments. Leukaphereses for immunogenicity testing were performed before the first (visit 12, referred to as 'pre-vaccination') and after the 8th vaccine injection (visit 20; referred to as 'post-vaccination').

Imaging of thorax, abdomen, brain by CT scans and MRI were performed at baseline (visit 1), pre-vaccination (visit 12), day 90 (visit 21) and at end of continued treatment (visit 26) according to the local imaging guidelines and RECIST version 1.1 and the immune-related response criteria (irRC) guideline[24]. Safety was characterized according to CTCAE v4.03 from grade 1 up to grade 5.

The data presented here are based on an exploratory interim analysis with a data cut-off date of November 2016.

Patient material and cell lines. Formalin-fixed and paraffin-embedded (FFPE) or fresh frozen tumour tissue was acquired at routine diagnostic resections and the tumour content was assessed in H&E-stained sections.

Fresh tumour samples were used for the preparation of tumour-infiltrating lymphocytes (TILs) and primary tumour cell lines.

TILs were grown from small pieces of fresh tumour tissue cultured in X-Vivo 15 medium (Lonza) with 2% human serum albumin (CSL-Behring) and 6,000 U ml^{-1} IL-2 (Proleukin S, Novartis) for two weeks as previously published[25]. Thereafter, TILs were expanded for two weeks using irradiated, allogeneic PBMCs as feeder cells in the presence of 30 ng ml^{-1} anti-CD3 IgG2a (clone OKT3, eBiosciences) and 300 U ml^{-1} IL-2 (Proleukin S, Novartis).

For the generation of patient-derived melanoma cell lines, fresh tumour tissue fragments were cultured in RPMI1640 medium (Life Technologies) supplemented with 15% FCS (Biochrome AG).

PBMCs obtained for immune monitoring or as starting material for the manufacturing process were isolated by Ficoll-Hypaque (Amersham Biosciences) density gradient centrifugation from buffy coats of healthy donors or from peripheral blood samples of melanoma patients. Immature DCs (DCs) were generated as described previously[26]. K562 cells (ATCC) were cultured under standard conditions. Cell banks were generated tested for mycoplasma. Reauthentication of cells was performed by short tandem repeat (STR) profiling at ATCC.

Next-generation sequencing. DNA was extracted from three 10-μm curls of FFPE tumour tissue in triplicate using a modified version of Qiagen's QIAamp DNA FFPE Tissue kit. RNA extraction from FFPE tumour curls was done in duplicates using Qiagen's RNeasy FFPE kit. For DNA and RNA extractions from fresh frozen tumour samples or cells, Qiagen's DNeasy Blood and Tissue Kit and RNeasy Mini Kit, respectively, were used.

Extracted nucleic acids were used for generation of various libraries. RNA-seq libraries were prepared in duplicate from FFPE tumour or cell line RNA using Illumina's TruSeq RNA Sample Prep kit V2 and 1 μg total RNA as input. DNA exome capture libraries were constructed in duplicates from 1 to 3 μg of FFPE tumour DNA and matching PBMC DNA using Agilent's SureSelect XT V4 Human All Exon.

NGS libraries for whole-genome sequencing of MZ-GaBa-018 and matching PBMCs were prepared by fragmenting 100 ng genomic DNA in a total volume of 15 μl using microTUBE-15 (Covaris Ltd) to an average fragment length of approximately 160 bp. The library was prepared with NEB's NEBNext Ultra DNA Library Prep Kit for Illumina using 25 ng of fragmented gDNA as input.

For NGS, the libraries were diluted to 2 nM or 10 nM and clustered at 10 pM using the Illumina TruSeq PE Cluster kit v3-cBot-HS. Each exome capture library was sequenced separately in one lane, whereas the RNA library replicates were sequenced as 2-plexes in one lane. All libraries were sequenced paired-end 50 nt on an Illumina HiSeq 2500 platform using two of Illumina's TruSeq SBS Kit v3-HS 50 cycles. MZ-GaBa-018 cell line and matching PBMC whole-genome sequencing libraries were spread over 4 lanes each and sequenced paired-end 100 nt on the same platform using Illumina TruSeq SBS Kit v3-HS 200 cycles.

Bioinformatics and mutation discovery. All mutanome-related data analysis steps for a single patient were coordinated by a software pipeline implemented in the Python programming language. For the DNA libraries, a minimum of 150×10^6 paired-end 50 nt reads and for the RNA libraries a minimum of 75×10^6 paired-end 50 nt reads were required.

For mutation detection, DNA reads were aligned to the reference genome hg19 with bwa[27]. Duplicate exomes from tumour and matched normal samples were analysed for single nucleotide variants. Loci with putative homozygous genotypes in the normal samples were identified and filtered to retain high confidence calls for single nucleotide variants. Remaining sites were further inspected for a putative homozygous or heterozygous mutational event. Suspected sites were filtered to remove potential false positives. Replicates were incorporated by testing both the sum of replicates and replicates separately. The final list of single-nucleotide variants was comprised of high confidence homozygous sites in the normal samples and high confidence heterozygous or homozygous mutational events in the tumour samples. Genomic coordinates of identified variants were compared with the UCSC known genes transcript coordinates in order to associate the variants with genes, transcripts, potential amino acid sequence changes and the RNA-seq-derived expression values.

For RNA-seq, RNA reads were aligned to the hg19 reference genome and transcriptome using bowtie[28], and gene expression was determined by comparison with UCSC known genes transcript and exon coordinates, followed by normalization to RPKM units[29].

Neo-epitope prioritization and selection. Generally speaking, two independent principles were applied to rank mutations. One used predicted high-affinity binding to the patient's HLA class II molecules combined with high expression levels of the mutation encoding RNA[2]. The other was based on predicted HLA class I binding. Mutated allele frequencies and relative transcription values served as further differentiators to prioritize mutations with comparable predicted HLA binding affinity. In more detail, the process was as follows:

From the identified single-nucleotide variants, up to 46 predicted variants were selected by an evolving procedure: (1) removal of non-sense variants and filtering by non-zero exon- and transcript expression; followed by sorting first by exon expression and then by HLA class I binding prediction score using a stable sorting algorithm and selecting up to 46 variants (P01–P04). (2) Removal of non-sense variants and filtering by non-zero exon- and transcript expression and non-zero variant frequency in the RNA-seq data; followed by sorting first by exon expression and then by HLA class I binding prediction score using a stable sorting algorithm and selecting up to 23 target peptide sequences; followed by sorting the remaining target peptide sequences first by HLA class I binding prediction score and then by exon expression using a stable sorting algorithm and selecting up to 23 additional target peptide sequences; both selection steps were not allowed to result in more than 46 selected variants (P05–P07, P09–P12); and (3) removal of non-sense variants and filtering by non-zero exon- and transcript expression and non-zero variant frequency in the RNA-seq data; followed by sorting first by exon expression and then by HLA class II binding prediction score using a stable sorting algorithm and selecting up to 20 target peptide sequences with gene expression ≥10 RPKM; followed by sorting the remaining target peptide sequences first by expression and then by HLA class I binding prediction score using a stable sorting algorithm and selecting up to 20 additional target peptide sequences; followed by sorting the remaining target peptide sequences first by HLA class I binding prediction score and then by exon expression using a stable sorting algorithm and filling up to 46 selected variants (P17, P19). The final selection of up to ten mutated target peptides per patient required the decision of a target selection board that evaluated the target peptides based on MHC I and MHC II binding predictions, gene expression and variant allele frequency.

HLA binding affinity was predicted via the IEDB-recommended mode of the IEDB T cell prediction tools[30] (version 2.5) using all variant-containing 8–11mers for HLA-A/B or 15-mers for HLA-DRB/DQB binding estimations. Out of all predictions for a single variant, the best consensus score was associated with the respective variants.

On the basis of these data, a short list of single-nucleotide variants were selected for confirmation by Sanger sequencing.

Sanger sequencing. For primer design, genomic sequences flanking the mutation sites were extracted from the reference genome and used as input for the primer3 software[31,32]. The output primer pairs were aligned to the reference genome using blast[33]. Primer pairs with alignments to off-target loci were removed and the remaining optimal primer pair was returned for each input site.

Sanger sequencing was performed by amplifying each selected mutated locus from tumour tissue and PBMC DNA by PCR (15 min at 95 °C for the initial activation followed by 35 cycles of 30 s at 94 °C for denaturation, 30 s at 60 °C for annealing, 30 s at 72 °C for extension, and 6 min at 72 °C for the final extension). Each PCR product was quality controlled using a QIAxcel (Qiagen) device and purified via ExoI/AP treatment or MinElute PCR Purification Kit (Qiagen). Sanger sequencing was performed by Eurofins/MWG Ebersberg, Germany.

Manufacturing of *in vitro* transcribed RNA. Synthetic DNA fragments coding for five putative neo-epitopes (each as 27mer with the mutation at position 14) connected by non-immunogenic glycine/serine linkers (start linker LQ for P01–P07 or GGSGGGGSGG, middle linker GGSGGGGSGG and end linker GGSLGGGGSG) were cloned into a starting vector, containing the SP- and MITD-domains[34] (SP, MRVTAPRTLILLLSGALALTETWAGS; MITD, IVGIVAGLAVLAVVVIGAVVATVMCRRKSSGGKGGSYSQAASSDSAQGSD VSLTA) for optimized routeing to HLA class I and II pathways and backbone sequence elements for improved RNA stability and translational efficiency[26]. The DNA was linearized, spectrophotometrically quantified, and subjected to *in vitro* transcription with T7 RNA polymerase as previously described[35] in the presence of 7.5 mM ATP, CTP, UTP, GTP and 3 mM β-S-ACA(D1) cap analogue[36] in a clean-room environment. RNA was purified using magnetic particles[37] and integrity was assessed by gel electrophoresis and microfluidic capillary electrophoresis (Experion, Biorad). Further analyses included determination of concentration, appearance, pH, osmolality, potency, endotoxin level and sterility.

***In vitro* stimulation of PBMCs.** $CD4^+$ and $CD8^+$ T cells were isolated from cryopreserved PBMCs using microbeads (Miltenyi Biotec). T cells, CD4- or CD8-depleted PBMCs were left to rest overnight. CD4- or CD8-depleted PBMCs were electroporated with RNA encoding patient-specific mutated targets, eGFP, influenza matrix protein 1 (M1) or tetanus p2/p16 sequences (positive control), left to rest for 3 h at 37 °C and irradiated at 15 Gy. $CD4^+$/$CD8^+$ T cells and electroporated and irradiated antigen-presenting cells were then combined at an effector to target ratio of 2:1. After one day, fresh culture medium containing 10 U ml^{-1} IL-2 (Proleukin S, Novartis) and 5 ng ml^{-1} IL-15 (Peprotech) was added. IL-2 was replenished 7 days after setting up the cultures. After 11 days of stimulation, cells were analysed via flow cytometry and used in ELISpot assays.

ELISpot. Multiscreen filter plates (Merck Millipore), pre-coated with antibodies specific for IFNγ (Mabtech) were washed with PBS and blocked with X-Vivo 15 (Lonza) containing 2% human serum albumin (CSL-Behring) for 1–5 h. 0.5–3 × 10^5 effector cells per well were stimulated for 16–20 h (40 h for TILs) with either autologous DCs electroporated with RNA or loaded with peptides, melanoma cell lines or HLA class I or II transfected K562 cells. For analysis of *ex vivo* T cell responses, cryopreserved PBMCs were subjected to ELISpot after a resting period of 2–5 h at 37 °C. All tests were performed in duplicate or triplicate and included assay positive controls (Staphyloccocus enterotoxin B (Sigma Aldrich)) as well as cells from a reference donor with known reactivity. Spots were visualized with a biotin-conjugated anti-IFNγ antibody (Mabtech) followed by incubation with ExtrAvidin-Alkaline Phosphatase (Sigma-Aldrich) and BCIP/NBT substrate (Sigma-Aldrich). Plates were scanned using CTL ImmunoSpot Series S five Versa ELISpot Analyzer (S5Versa-02-9038) and analysed by ImmunoCapture V6.3 software. Spot counts were summarized as median values for each triplicate. T cell responses stimulated by mutated RNA or peptides were compared to control RNA (luciferase) electroporated target cells or unloaded target cells, respectively. A response was defined as positive with a minimum of five spots per 1 × 10^5 cells in the *ex vivo* setting or 25 spots per 5 × 10^4 cells in the post-IVS setting as well as a spot count that was more than twice as high as the respective control.

Multimer staining and data analysis. Mutation-specific $CD8^+$ T cells were identified using dextramers (Immudex) carrying nine- or ten-amino-acid-long epitopes from immunogenic mutations. Cells were first stained with multimers, after which staining of cell surface markers (CD28 CD28.8, CD197 150503, CD45RA HI100, CD3 UCHT1, CD16 3G8, CD14, MΦP9, CD19 SJ25C1, CD27 L128, CD279 EH12, CD8 RPA-T8 all BD and CD4 OKT4 Biolegend) and live-dead staining (DAPI BD) was performed. The stained cells were then acquired on a BD LSR Fortessa SORP. Singlet, live, multimer-positive events were identified within CD3- (or CD8) positive, CD4/CD14/CD16/CD19-negative or CD3- (or CD8) positive/CD4-negative events. The specificity of HLA-A*0201 dextramers for patient-specific neo-epitopes is demonstrated by lack of staining of HLA-A*0201^+ blood donors (Extended Data Fig. 6c).

Intracellular cytokine staining. Autologous DCs electroporated with RNA encoding single neo-epitopes were added at a 10:1 effector:target ratio and cultured for about 16 h at 37 °C in the presence of Brefeldin A and Monensin. Cells were stained for viability (fixable viability dye eFluor506, eBioscience), followed by staining for surface markers (CD8 SK1 BD, CD4 OKT4, Biolegend). After permeabilization, intracellular cytokine staining was performed (IL-2 MQ1-17H12, IFNγ B27 all BD and TNFα Mab11 Biolegend) and the samples were acquired on a BD FACS Canto II (Becton Dickinson).

Single-cell sorting. Sorting of single-antigen-specific T cells was conducted after 11 days of antigen-specific expansion of PBMCs, purified $CD8^+$ or $CD4^+$ T cells or TILs. Before sorting, 2 × 10^6 expanded T cells were restimulated with 2 × 10^5 autologous DCs transfected with IVT RNA encoding the respective neo-antigen or a control antigen. After 16 to 20 h, cells were collected and treated with fluorochrome-conjugated antibodies directed against CD14, CD19, CD3, CD8, CD4, CD137 and CD134 (all from BD Biosciences), as well as IFNγ using the IFNγ secretion assay kit (Miltenyi Biotec). Sorting of single-neo-antigen-specific T cells was conducted on a BD FACS Aria flow cytometer (BD Biosciences). One double-positive cell (IFNγ/CD8, CD137/CD8, IFNγ/CD4 or CD134/CD4) per well was collected in a 96-well V-bottom-plate (Greiner Bio-One) containing 3T3-L1 carrier cells, centrifuged and stored at −65 °C to −85 °C.

Cloning of neo-epitope-specific TCRs. Cloning of TCR genes from single T cells was performed as previously described[38]. In brief, total RNA extracted with the Micro RNeasy Kit (Qiagen) was used for template-switch cDNA synthesis with RevertAid H Minus Reverse Transcriptase (Thermo Fisher) followed by preamplification using PfuUltra Hotstart DNA Polymerase (Agilent). Aliquots of the resulting cDNAs were used for Vα/Vβ gene-specific multiplex PCRs. Products were analysed on a capillary electrophoresis system (Qiagen). Samples with bands at 430–470 bp were size-fractionated on agarose gels and the bands excised and purified using a Gel Extraction Kit (Qiagen). Purified fragments were sequenced and the respective V(D)J junctions analysed using the IMGT/V-Quest tool[39]. DNAs of novel and productively rearranged corresponding TCR chains were NotI-digested and cloned into pST1 vectors containing the appropriate backbones for *in vitro* transcription of complete TCR-α/β chains[38].

TCR-α/β deep sequencing was performed with total RNA from PBMCs using the TCR-Typer kit (BioNTech Diagnostics). The resulting DNA libraries were sequenced on an Illumina MiSeq sequencer using 2 × 300 bp paired-end chemistry. Sequencing data were analysed with Typer Toolbox software. The number of total TCR reads per sample ranged from 1.1 × 10^6 to 1.5 × 10^6.

qRT–PCR. RNA and cDNA were generated with the ExpressArt FFPE Clear RNAready kit (AmpTec) and PrimeScript RT Reagent Kit with gDNA Eraser (Takara Bio Inc.), respectively. qRT–PCR was performed using the BioMark HD system (Fluidigm) or the 96-well Applied Biosystems 7300 Real-Time PCR System. Samples and assays were prepared and analysed according to the 'Fast Gene Expression Analysis' from FFPE-derived RNA using Quantitative SYBR Green Real-Time PCR or TaqMan Gene Expression Assays on the BioMark or 'BioMark HD System Fluidigm' Advanced Development Protocol 28. 96.96 Gene Expression Dynamic Array IFCs were loaded using the IFC Controller HX.

Immunohistochemistry. After deparaffinization of 3–4-μm FFPE sections, slides were subjected to antigen retrieval by boiling in 10 mM citric acid supplemented with 0.05% Tween-20 (pH 6.0) at 120 °C for 10 min, subsequently quenched (by 0.3% H_2O_2; 15 min) and blocked with 10% goat serum in PBS (30 min) at room temperature.

Slides were incubated overnight at 2–8 °C with 0.2 μg ml^{-1} anti-human CD3 (F7.2.38; Dako), 0.2 μg ml^{-1} anti-human CD8 (C8/144B; Dako), 1 μg ml^{-1} anti-human FoxP3 (236A/E7; Abcam), 1:200 anti-PD-L1 (13684; Cell Signaling Technologies) or 1:2,500 anti-β2-microglobulin (D8P1H; Cell Signaling Technologies) in blocking buffer. Antibody binding was visualized with horseradish-peroxidase-labelled secondary antibodies (BrightVision HRP, Immunologic) together with a red substrate–chromogen solution (VectorRed; Vector Labs). Tumour cells were stained with 1 μg ml^{-1} of a Melan-A-specific antibody (A103, Dako).

Sections were subsequently counter-stained with Mayer's haematoxylin (Carl Roth GmbH) and subjected to evaluation by a computer based analysis (Definiens Developer).

For analysis, slides were scanned (Axio Scan, Zeiss) and manually pre-defined tumour, normal tissue and necrotic areas were quantified via computerized image analysis software (Developer, Definiens). The number of $CD3^+$, $CD8^+$ and $FOXP3^+$ TILs was determined in the areas classified as tumour tissue.

Characterization of B2M loss in patient P04. RNA expression levels of HLA class I and β2-microglobulin were determined in the RNA-seq data of the cell line MZ-GaBa-018. The deletion of the *B2M* locus was detected by the manual curation of the exome alignments of MZ-GaBa-018 in the Integrative Genomics Viewer[40] (IGV) and the deletion start point upstream of *B2M* was defined. The deletion end point was deduced by split read and discordant paired-end alignments. In addition, exome reads were applied to *de novo* assembly using Trinity[41].

Cloning of HLA antigens. HLA antigens were synthesized by a service provider (Eurofins Genomics) according to respective high-resolution HLA typing results. *HLA-DQA* sequences were amplified from donor-specific cDNA with 2.5 U

plaque-forming units of polymerase using the forward primer DQA1_s (PHO-GCCACCATGATCCTAAACAAAGCTCTGMTGC) and the reverse primer DQA1_as (TATGCGATCGCTCACAAKGGCCCYTGGTGTCTG). HLA antigens were cloned into appropriately digested IVT vectors[38].

RNA transfer into cells. RNA was added to cells suspended in X-Vivo 15 medium (Lonza) in a precooled 4-mm gap sterile electroporation cuvette (Bio-Rad). Electroporation was performed with a BTX ECM 830 Square Wave Electroporation System (T cells: 500 V, 3 ms, 1 pulse; iDC: 300 V, 12 ms, 1 pulse; bulk PBMCs: 400 V, 6 ms, 1 pulse; MZ-GaBa-018: 225 V, 3 ms, 2 pulses; K562: 200 V, 8 ms, 3 pulses).

Peptides. Synthetic 15mer peptides with 11 amino acid overlaps covering the 27mer neo-antigen sequences (4 OLPs per neo-antigen) or control antigens (HIV-gag, TPTE), referred to as overlapping peptide pools (OLP), or 8–11mer epitopes were used. All synthetic peptides were purchased from JPT Peptide Technologies GmbH and dissolved in AquaDest. (Aqua B. Braun, BRAUN Melsungen) with 10% DMSO to a final concentration of 3 mM.

Flow cytometric analyses. Cell surface expression of transfected TCR genes was analysed by flow cytometry using PE- or FITC-conjugated anti-TCR antibodies against the appropriate variable region family or the constant region of the TCR-β chain (Beckman Coulter) and FITC- or APC-labelled anti-CD8/CD4 antibodies (BD Biosciences). HLA antigens of the antigen-presenting cells used for evaluating the function of TCR-transfected T cells were detected by staining with FITC-labelled HLA class II-specific (Beckman Coulter) and PE-labelled HLA-class-I-specific antibodies (BD Biosciences). Flow cytometric analysis was performed on a BD FACSCanto II analytical flow cytometer (BD Biosciences). Acquired data were analysed using version ten of the FlowJo software (Tree Star).

Cytotoxicity assay. A luciferase-based cytotoxicity assay was performed as previously described[42]. 1×10^4 target cells transfected either with luciferase RNA alone or in combination with *B2M* RNA were co-cultured with mutation-specific effector T cells (either OKT3-activated TCR-transfected $CD8^+$ T cells or $CD4^+$/$CD8^+$ IVS T cells) for 19 to 25 h. A reaction mixture containing D-Luciferin (BD Biosciences; final concentration, 1.2 mg ml^{-1}) was added. One hour later, luminescence was measured using a Tecan Infinite M200 reader (Tecan). Cell killing was calculated by measuring the reduction of total luciferase activity. Viable cells were measured by the luciferase-mediated oxidation of luciferin. Specific killing was calculated according to the following equation:

$$\text{Specific killing in \%} = 100 - \left(\frac{(\text{sample} - \text{complete lysis})}{(\text{max . viable cells} - \text{complete lysis})} \times 100 \right)$$

Apoptosis assay. For caspase-3/7 activation apoptosis assay (IncuCyte), 1×10^4 melanoma cells and 20×10^4 effector T cells were plated per well in 96-well Corning plates for 24 h. Caspase-3/7 reagent was added at a 1:1,000 dilution of a 5 mM stock solution (Essen Bioscience), each condition in triplicate. Cells were imaged at tenfold magnification in an IncuCyte Zoom Live-content imaging system (Essen Bioscience) at 37 °C, 5% CO_2. Images were acquired every hour for 24 h, four images per well. Data were analysed using IncuCyte analysis software to detect and quantify green (apoptotic) cells per image. Average number of green spots determined from triplicate measurements after an 8.5 h co-culture with error bars corresponding to standard deviations were plotted using GraphPad Prism software.

Data availability. All data are available from the authors on reasonable request.

24. Wolchok, J. D. *et al.* Guidelines for the evaluation of immune therapy activity in solid tumors: immune-related response criteria. *Clin. Cancer Res.* **15,** 7412–7420 (2009).
25. Dudley, M. E., Wunderlich, J. R., Shelton, T. E., Even, J. & Rosenberg, S. A. Generation of tumor-infiltrating lymphocyte cultures for use in adoptive transfer therapy for melanoma patients. *J. Immunother.* **26,** 332–342 (2003).
26. Holtkamp, S. *et al.* Modification of antigen-encoding RNA increases stability, translational efficacy, and T-cell stimulatory capacity of dendritic cells. *Blood* **108,** 4009–4017 (2006).
27. Li, H. & Durbin, R. Fast and accurate short read alignment with Burrows–Wheeler transform. *Bioinformatics* **25,** 1754–1760 (2009).
28. Langmead, B., Trapnell, C., Pop, M. & Salzberg, S. L. Ultrafast and memory-efficient alignment of short DNA sequences to the human genome. *Genome Biol.* **10,** R25 (2009).
29. Mortazavi, A., Williams, B. A., McCue, K., Schaeffer, L. & Wold, B. Mapping and quantifying mammalian transcriptomes by RNA-seq. *Nat. Methods* **5,** 621–628 (2008).
30. Kim, Y. *et al.* Immune epitope database analysis resource. *Nucleic Acids Res.* **40,** W525–W530 (2012).
31. Untergasser, A. *et al.* Primer3—new capabilities and interfaces. *Nucleic Acids Res.* **40,** e115 (2012).
32. Koressaar, T. & Remm, M. Enhancements and modifications of primer design program Primer3. *Bioinformatics* **23,** 1289–1291 (2007).
33. Kent, W. J. BLAT—the BLAST-like alignment tool. *Genome Res.* **12,** 656–664 (2002).
34. Kreiter, S. *et al.* Increased antigen presentation efficiency by coupling antigens to MHC class I trafficking signals. *J. Immunol.* **180,** 309–318 (2008).
35. Grudzien-Nogalska, E. *et al.* Synthetic mRNAs with superior translation and stability properties. *Methods Mol. Biol.* **969,** 55–72 (2013).
36. Kuhn, A. N. *et al.* Phosphorothioate cap analogs increase stability and translational efficiency of RNA vaccines in immature dendritic cells and induce superior immune responses in vivo. *Gene Ther.* **17,** 961–971 (2010).
37. Berensmeier, S. Magnetic particles for the separation and purification of nucleic acids. *Appl. Microbiol. Biotechnol.* **73,** 495–504 (2006).
38. Simon, P. *et al.* Functional TCR retrieval from single antigen-specific human T cells reveals multiple novel epitopes. Cancer *Immunol. Res.* **2,** 1230–1244 (2014).
39. Brochet, X., Lefranc, M.-P. & Giudicelli, V. IMGT/V-QUEST: the highly customized and integrated system for IG and TR standardized V-J and V-D-J sequence analysis. *Nucleic Acids Res.* **36,** W503–W508 (2008).
40. Thorvaldsdóttir, H., Robinson, J. T. & Mesirov, J. P. Integrative Genomics Viewer (IGV): high-performance genomics data visualization and exploration. *Brief. Bioinform.* **14,** 178–192 (2013).
41. Zhao, Q.-Y. *et al.* Optimizing *de novo* transcriptome assembly from short-read RNA-Seq data: a comparative study. *BMC Bioinformatics* **12** (Suppl 14), S2 (2011).
42. Omokoko, T. A. *et al.* Luciferase mRNA transfection of antigen presenting cells permits sensitive nonradioactive measurement of cellular and humoral cytotoxicity. *J. Immunol. Res.* **2016,** 9540975 (2016).